iScience

CellPress
OPEN ACCESS

Article

Engineering a versatile and retrievable cell macroencapsulation device for the delivery of therapeutic proteins

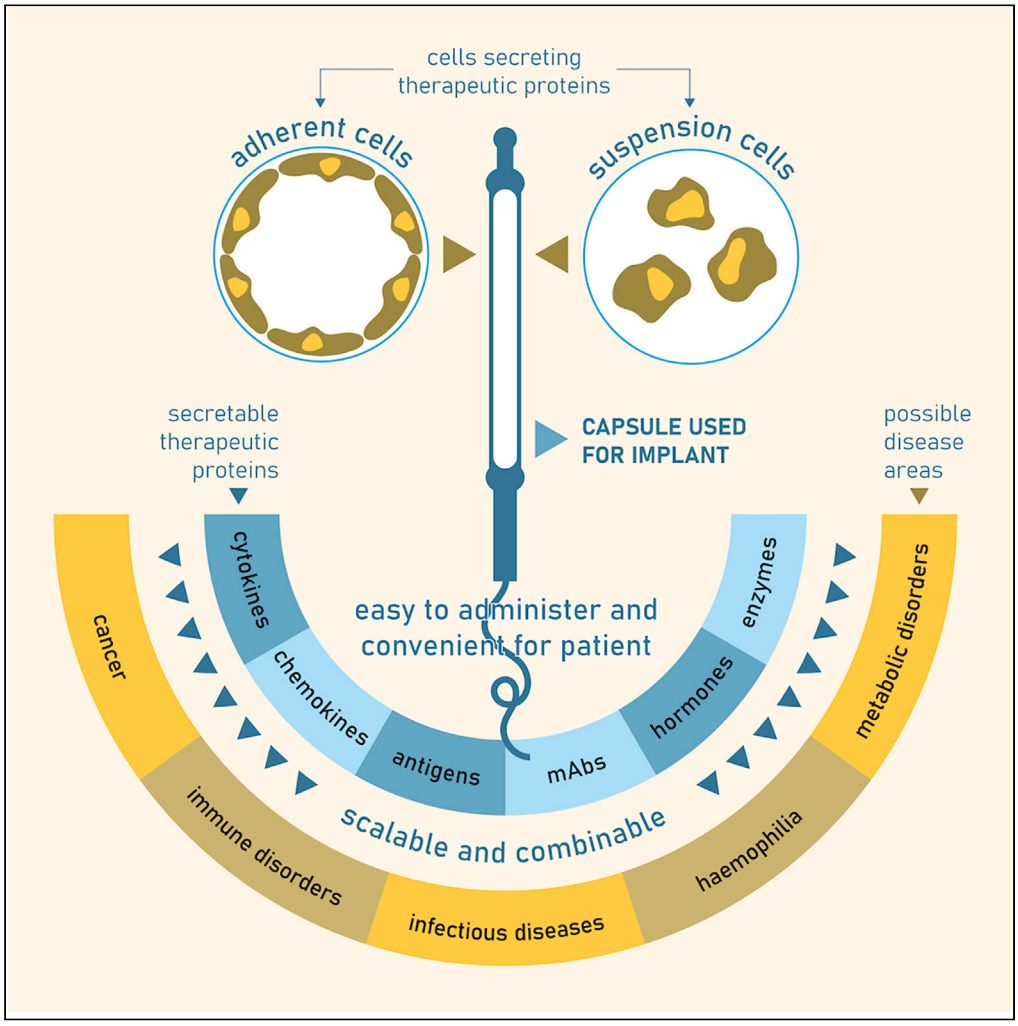

Julien Grogg, Remi Vernet, Emily Charrier, ..., Nicolas Gaudenzio, Adrien Engel, Nicolas Mach

jgrogg@maxivax.ch

Highlights

A versatile cell macroencapsulation device for *in vivo* protein delivery

Different cell lines secreting different proteins can be combined in the device

No burdensome surgery required for both implantation and retrieval of the device

Many potential clinical applications including cancer immunization therapies

Grogg et al., iScience *26*, 107372
August 18, 2023
https://doi.org/10.1016/j.isci.2023.107372

iScience

CellPress
OPEN ACCESS

Article

Engineering a versatile and retrievable cell macroencapsulation device for the delivery of therapeutic proteins

Julien Grogg,[1,2,3,7,*] Remi Vernet,[1,2] Emily Charrier,[1,2,3] Muriel Urwyler,[1,2] Olivier Von Rohr,[1,2] Valentin Saingier,[1,2] Fabien Courtout,[1,2] Aurelien Lathuiliere,[4] Nicolas Gaudenzio,[5,6] Adrien Engel,[1,2,3] and Nicolas Mach[1,2]

SUMMARY

Encapsulated cell therapy holds a great potential to deliver sustained levels of highly potent therapeutic proteins to patients and improve chronic disease management. A versatile encapsulation device that is biocompatible, scalable, and easy to administer, retrieve, or replace has yet to be validated for clinical applications. Here, we report on a cargo-agnostic, macroencapsulation device with optimized features for protein delivery. It is compatible with adherent and suspension cells, and can be administered and retrieved without burdensome surgical procedures. We characterized its biocompatibility and showed that different cell lines producing different therapeutic proteins can be combined in the device. We demonstrated the ability of cytokine-secreting cells encapsulated in our device and implanted in human skin to mobilize and activate antigen-presenting cells, which could potentially serve as an effective adjuvant strategy in cancer immunization therapies. We believe that our device may contribute to cell therapies for cancer, metabolic disorders, and protein-deficient diseases.

INTRODUCTION

Encapsulated cell therapy (ECT) consists of encasing living cells within an immunoprotective, selectively permeable membrane. It is an effective way of delivering therapeutic proteins released by genetically engineered cells to target a specific disease.[1] Over the last two decades, ECT has been investigated in many preclinical and clinical models, leading to an evolution of the technology along with the foundation of tangible clinical applications.[2,3] The latter includes type 1 diabetes, neurodegenerative disease and pain, acute liver failure, cancer, hypoparathyroidism, chronic eye diseases, wound healing and regeneration, kidney failure, metabolic disorders, and cardiovascular diseases.[4–7] The use of ECT for therapeutic protein delivery has significant advantages, such as preventing repetitive administrations in the treatment of chronic diseases or during protein replacement therapy. It combines the potency of *de novo in situ* synthesis of cell-derived therapeutic proteins and peptides with the safety of an implantable and retrievable medical device.[8] By locally delivering the active protein, it may achieve efficacy while circumventing systemic toxicities in certain indications.[9] The technology relies essentially on two elements: the encapsulation vehicle and the transplanted cells. Cells can be microencapsulated; i.e., encased as single cells or clusters of cells in a polymeric membrane or matrix of a micron-range thickness,[10–12] or macroencapsulated; i.e., large groups of cells housed in a device.[13–15] One of the major limitations of microencapsulation is the degradation of the polymer matrix and additives over time, in response to heat, hydrolysis, and biological agents.[16] This has a negative impact on the core particle's stability as well as the surrounding tissues.[17] We focused on the development of a macroencapsulation device with robust mechanical stability, better suited for longer-term protein delivery. In addition, macrocapsules can be retrieved, which makes the therapy fully reversible in case of loss of function or adverse events, and significantly mitigates safety risks compared to microencapsulation strategies.[18–20] We distinguish two main designs of macroencapsulation devices: flat sheet devices, such as the commercially available TheraCyte; and hollow fiber devices, which are cylindrical in shape. In both designs, the size-selective permeability of the membrane allows a bidirectional molecular exchange between the inner and outer environments. Such exchange includes the inward diffusion of nutrients, trophic factors and oxygen, essential for the survival of encapsulated cells, and the passive diffusion of secretomes, such as the therapeutic protein and metabolites produced by the encapsulated cells. The membrane also serves as a physical barrier between the loaded cells and the host's immune cells, allowing the survival of cells from allogeneic and

[1]Department of Oncology, Geneva University Hospitals and Medical School, 1211 Geneva, Switzerland

[2]Centre for Translational Research in Onco-Hematology, Oncology Division, Geneva University Hospital and University of Geneva, Geneva, Switzerland

[3]MaxiVAX SA, Geneva, Switzerland

[4]Department of Rehabilitation and Geriatrics, University of Geneva, 1211 Geneva, Switzerland

[5]Toulouse Institute for Infectious and Inflammatory Diseases (Infinity) INSERM UMR1291 - CNRS UMR5051 - University Toulouse III, Toulouse, France

[6]Genoskin SAS, Toulouse, France

[7]Lead contact

*Correspondence: jgrogg@maxivax.ch

https://doi.org/10.1016/j.isci.2023.107372

xenogeneic sources.[19,21] Depending on the permeability of the membrane, large molecules produced by host immune cells, such as antibodies, could diffuse into the capsule and potentially react against encapsulated cells. To mitigate immune reaction from the host, the device should be highly biocompatible and the encapsulated cells as minimally immunogenic as possible.

Our group first developed MVX-ONCO-1, a therapeutic cancer vaccine relying on ECT to deliver the adjuvant to the immunization site.[22–24] Building on the experience gathered during the preclinical and clinical development of the MVX-ONCO-1 device (NCT02193503, NCT02999646), we designed the Myo-P device.[25,26] It addresses the weaknesses identified in MVX-ONCO-1's device (GEN-1), and broadens the scope of therapeutic applicability. The Myo-P device bears optimized features for clinical applications. These features include: a medical grade hollow fiber membrane (HFM) with a molecular weight cut-off (MWCO) that allows the release of complex proteins by the encapsulated cells as well as a better exchange between the inner and the outer environments of the capsule; an internal matrix composed of clinical grade polyester yarns,[27] allowing adherent cells to attach, and optimizing spatial distribution; a built-in polypropylene retrieval thread embedded in the retrieval tube, allowing the extraction of implanted capsules; and a light-curable biocompatible adhesive with a lower shrinkage index and higher flexibility to reduce the mechanical tensions on the membrane caused by the curing,[28] without jeopardizing the robustness of the capsule. The increased flexibility also improves the overall *in vivo* robustness of the device.[29] All materials were selected on the basis of their biocompatibility and performance properties. The overall geometry of the device was also developed to favor biocompatibility and performance.[30] It achieves appropriate cellular density and consequently fosters cell survival and sustained production of therapeutic protein. Its cylindrical architecture also allows the device to be easily administered and retrieved, without any surgical procedures.[24]

We first assessed the safety and performance of the Myo-P device against the GEN-1 device. We also assessed its suitability to be loaded with both suspension and adherent cells. We explored its versatility by encapsulating a combination of different secreting cell lines and measuring its secretion capability both *in vitro* and *in vivo*. And finally, we assessed the potential cancer vaccine adjuvant application of the Myo-P device loaded with a cytokine (GM-CSF) secreting cell line. Our results support its effectiveness as a vehicle for different cell types and its potential contribution to cell therapies aiming at delivering proteins in various indications.

RESULTS

Engineering and development of the Myo-P device

The Myo-P device was specifically designed to encapsulate protein-secreting cells for subsequent implantation in patients (Video S1). It is an evolution of the GEN-1 device, which was successfully tested in 50 patients, in MVX-ONCO-1 Phase I and Phase IIa studies.[24] The Myo-P bears optimized features for ECT. These features extend its scope of use to a broad therapeutic applicability and also addresses weaknesses identified in the previous design. The key developments include an HFM with an MWCO, allowing for the release of large and complex proteins, such as antibodies, by the encapsulated cells, as well as a better exchange between the inner and outer environments of the capsule without compromising the viability of the cargo during implantation. The GEN-1 device's HFM limits this delivery to molecules with a size of 100 kDa or less. The Myo-P membrane was selected on the basis of its porosity (0.65 μm) and its mechanical properties to prevent any structural impairment. Illustrations of the membranes and uniform macroporous surface of both the GEN-1 and the Myo-P membrane are depicted in Figures 1A and 1B. Another feature of the device is its capacity to be loaded with both adherent and suspension cells. To support such capacity, a specific substrate must be included in the cargo section of the capsule[31,32]; thus an internal matrix composed of clinical grade polyester yarns was integrated in the design of the Myo-P. The polyester yarns were placed longitudinally inside the reinforcement coil of the membrane (Figure 1C). The key physical specifications of the GEN-1 and the Myo-P membranes are described in Table S1. A built-in polypropylene thread embedded in the proximal glue point of the retrieval tube replaced the hook in the GEN-1 device to provide physicians with a ready-to-use device (Figures 1A and 1B). The demonstration of the quick and easy ambulatory administration of the GEN-1 device subcutaneously in a patient from the Phase I study of MVX-ONCO-1 (NCT02193503) is depicted in Figure 1D. The administration procedure of the Myo-P device will remain identical. During a simulated loading of cells, the transmembrane flow pressure remained below 1N in the Myo-P device, while it gradually increased to reach more than 6N in the GEN-1 device (Figure 2B). This indicates that a lower mechanical stress is applied on the cells during the loading in the Myo-P device. Both the Myo-P and the GEN-1 membranes support more than 2N of tensile strength. The absolute tensile strength difference is not

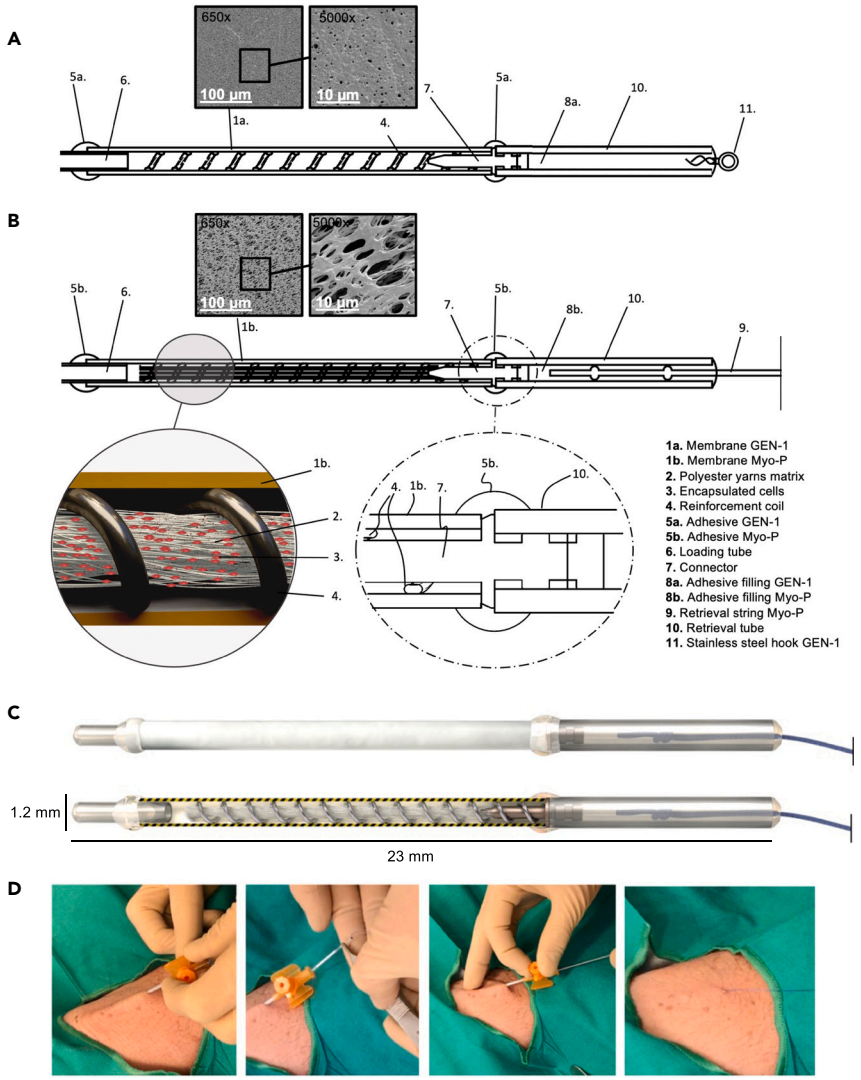

Figure 1. Design of the Myo-P device with optimized features for protein delivery in humans

(A and B) Schematic illustration of the GEN-1 device used in MVX-ONCO-1 (A) and the Myo-P device (B) with SEM images of the membranes and uniform macroporous surface.

(C) 3D illustrations of the Myo-P device with an internal view of the cargo section and the polyester (PET) yarn matrix.

(D) Demonstration of rapid device administration subcutaneously in a patient from the Phase I study with the GEN-1 device. The administration procedure of the Myo-P device remains identical.

See also Table S1.

mechanically meaningful toward *in vivo* residence as the tension on the membrane per se is minimal by design, even at retrieval: in the two clinical studies of MVX-ONCO-1, over 600 GEN-1 devices were subcutaneously implanted and retrieved from patients without any damage observed on the membrane. The variability at break is significantly lower with the Myo-P membrane (2.01–2.50) than with the GEN-1 membrane (2.2–3.5) (Figure 2C) which advocates for a well-controlled manufacturing process by the supplier of Myo-P membrane. The Myo-P membrane was shown to have more elasticity than the GEN-1 membrane (Figure 2D) as demonstrated by the superior angle at plastic deformation. A light-curable biocompatible adhesive with a lower shrinkage index and higher flexibility was also integrated into the design of the Myo-P. The adhesive used in the GEN-1 device (MD1180) was tested to assemble the Myo-P, and its curing created visible cracks in the membrane, damaging its mechanical integrity beyond acceptance. The adhesive (MD1187) reduces the mechanical tensions on the mPES membrane caused by the curing, without jeopardizing the robustness of the capsule (Figure 2A). A risk assessment was performed to identify potential criticality throughout the

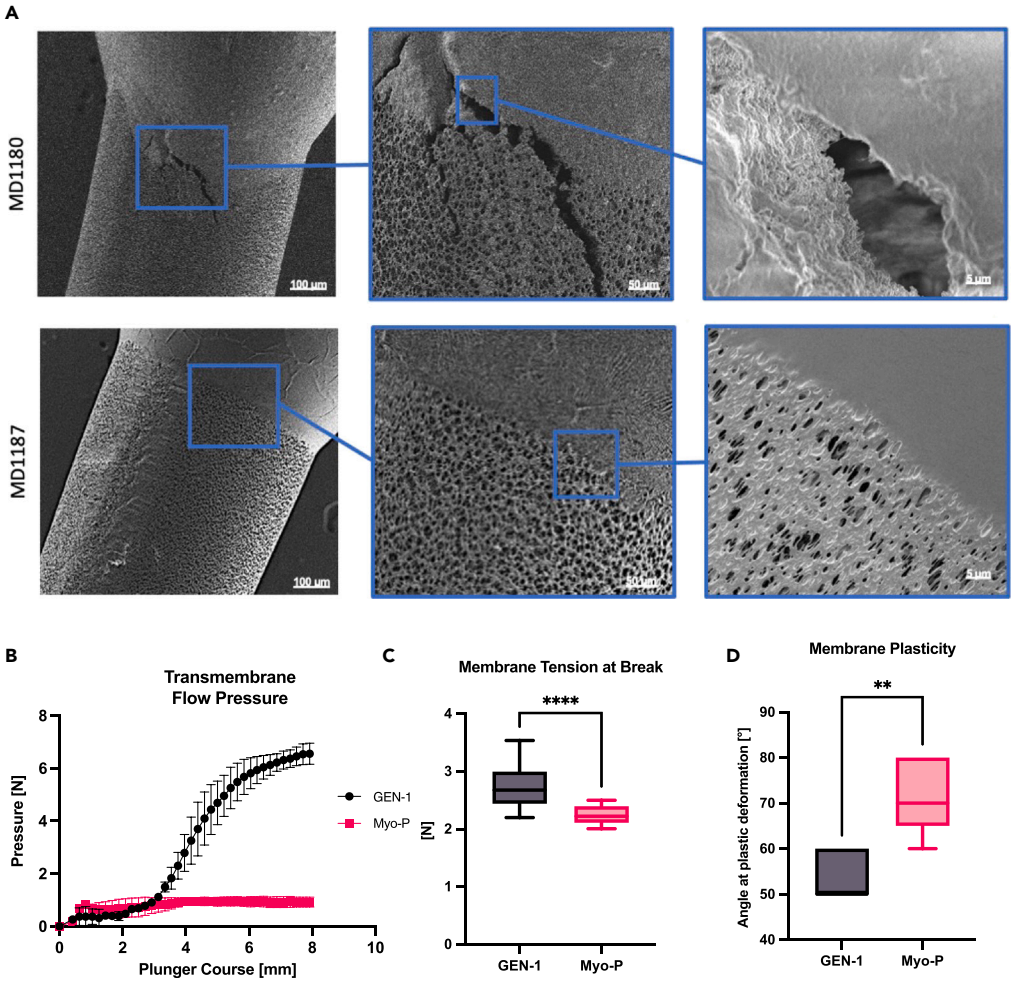

Figure 2. Mechanical characterization of the Myo-P device versus GEN-1 device

(A) SEM images of the Myo-P device after distal sealing with MD1180 and MD1187 adhesives, respectively.

(B–D) Characterization of the transmembrane flow properties and mechanical robustness of the Myo-P device in comparison to the GEN-1 device: (B) transmembrane flow pressure test (n = 3), (C) membrane tension at break (n = 20), and (D) membrane plasticity (n = 5). ** means significant difference (t-test) and $p < 0.01$; **** means significant difference and $p < 0.0001$.

See also Table S2.

manufacturing process of the Myo-P. The in-process and final controls implemented to mitigate the identified risks are listed in Table S2.

Performance and functional characterization of the Myo-P device for protein delivery

A huGM-CSF-secreting cell line (K562 cells)[22] was encapsulated at the same concentration in the GEN-1 device, and in the Myo-P device respectively, and devices were subsequently implanted in the subcutaneous tissue of C57/BL6 mice for one week (Figures 3A–3D). Prior to implantation, the mean huGM-CSF secretion was 98 ng/24 h/capsule in the GEN-1 device, and 149 ng/24 h/capsule in the Myo-P device. After explantation, the mean GM-CSF secretion was 28 ng/24 h/capsule in the GEN-1 device, and 137 ng/24 h/capsule in the Myo-P device. In the adjacent tissue, the mean GM-CSF concentration was 275 pg/mg of protein in the GEN-1 device, and 1195 pg/mg of protein in the Myo-P device. In the serum, the mean GM-CSF level was 35 pg/mL in the GEN-1 device, and 600 pg/mL in the Myo-P device. Overall secretion, serum and tissue concentration results support the superior protein delivery performance of the Myo-P device over its predecessor. In another experiment, we maintained Myo-P devices containing human myoblast cells secreting huGM-CSF (MVX-2/CCOS1901) in culture for 33 months, and the secretion of

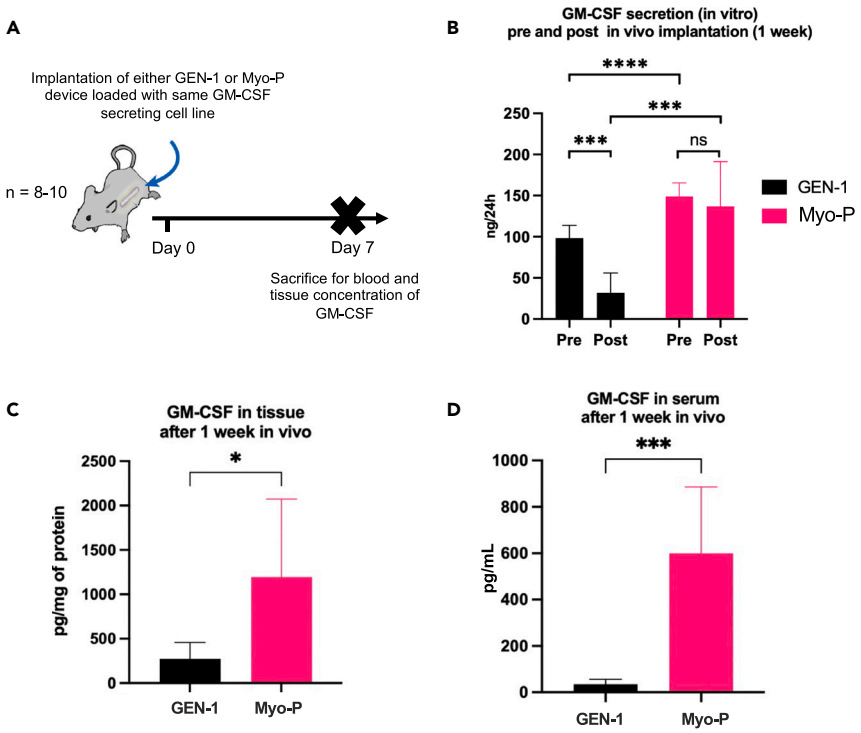

Figure 3. Performance characterization of the Myo-P device versus GEN-1 device

HuGM-CSF-secreting K562 cells (1M) were encapsulated in the GEN-1 device and in the Myo-P device, respectively. Devices were subsequently implanted into C57BL/6 mice and kept for one week in the mice.

(A) Scheme of the experimental procedure used to generate figures B–D.

(B) Prior to implantation, a 24-h release was performed to measure the huGM-CSF secretion by ELISA. Capsules were explanted after one week, and the day after the explantation, a 2-h release was performed to measure the huGM-CSF secretion by ELISA.

(C) Samples of tissue adjacent to the capsule were collected to quantify huGM-CSF levels.

(D) Serum samples were collected from implanted mice to quantify huGM-CSF levels.

(B–D) Each bar represents mean ± SD of n = 8–10 replicates. * means significant difference (t-test) and $p < 0.05$; *** means significant difference and $p < 0.001$; **** means significant difference and $p < 0.0001$.

huGM-CSF in culture supernatant ranged from 613 to 1173 ng/24 h/capsule over time (Figure 4A). We previously showed that Myo-P encapsulated huGM-CSF and anti-CD20 antibody-secreting cells implanted in the subcutaneous tissue of Rag2/IL2rg−/− mice produced both proteins to a measurable extent in the serum over 43 weeks[33] The latter model does not develop functional B, T, and NK cells, which results in a deficient adaptive immune response. It was selected to mitigate the effect of xenogeneic engineered transplanted cells on the immune system and avoid a neutralizing anti-drug response that may have altered the blood level of delivered recombinant protein.[34,35] Finally, we examined the impact of our standardized freezing and thawing procedures on the potency of MVX-2-loaded Myo-P devices (Myo-P2) (Figure 4B). A batch of 24 capsules was split into two sub-batches of 12 capsules. In the first sub-batch, the capsules were frozen and thawed, whereas in the second sub-batch, capsules were kept in culture. The freezing medium was specifically developed to be used with our device, as dimethyl sulfoxide, which is the usual cell cryoprotectant of choice, damages the membrane. The huGM-CSF secretion from both frozen and non-frozen encapsulated MVX-2 cells was comparable, ranging between an average of 900 ng/24 h/capsule and 2300 ng/24 h/capsule at all timepoints. These results suggest that both small (cytokines) and large molecules (antibodies) can be secreted by Myo-P encapsulated cells for several months, and that Myo-P encapsulated cells secretion is not hampered post-freezing.

Versatility of the Myo-P device

Myo-P devices were simultaneously loaded with a combination of two different cell lines stemming from the same parental lineage (IHM-2/CCOS1902). Wild type (WT) cells, huGM-CSF-secreting (MVX-2/CCOS1901)

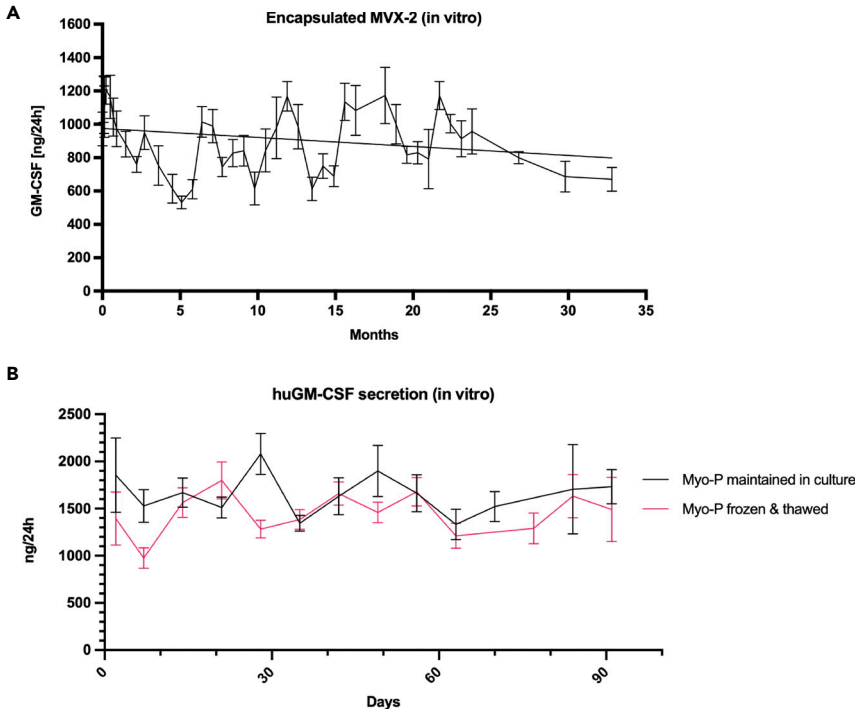

Figure 4. Functional characterization of the Myo-P device for sustained protein delivery and clinical translatability

(A) Devices containing MVX-2 cells were maintained in culture for 33 months, and the expression of huGM-CSF was quantified by ELISA over time. Each dot represents mean ± SD of n = 7 replicates.

(B) MVX-2 cells were either encapsulated and immediately maintained in culture for 90 days, or encapsulated, frozen and thawed, then subsequently maintained in culture for 90 days. The expression of huGM-CSF was quantified by ELISA over time. Each dot represents mean ± SD of n = 12 replicates. See also Table S3.

cells, and anti-CTLA4 antibody-secreting (MVX-3) cells were encapsulated either alone or in pairs, at defined concentrations. Devices were maintained in culture for 21 days, and the expression of huGM-CSF and anti-CTLA4 antibody was quantified by ELISA over time (Figures 5F and 5G). Myo-P devices loaded with 1 M of MVX-2 cells produced an average of 945 ng/24 h/capsule on Day 1 and reached a plateau from seven days onwards (1448 ng/24 h/capsule at Day 7 and 1483 ng/24 h/capsule on Day 21). Myo-P devices loaded with half the MVX-2 cells (0.5 M) produced on average approximatively half of the huGM-CSF (423 ng/24 h/capsule) on Day 1 compared to the ones loaded with 1 M of MVX-2 cells. Their production capabilities progressively increased to reach an average of 1405 ng/24 h/capsule at Day 21, which is the same level as the Myo-P devices loaded with 1 M of MVX-2 cells. The same trend was observed in Myo-P devices loaded with two different cell lines: 0.5 M of MVX-2 cells with either 0.5 M of MVX-3 or 0.5 M of WT cells. At Day 1, the average GM-CSF secretion level was 436 ng/24 h/capsule in the MVX-2+WT group, and 457 ng/24 h/capsule in the MVX-2+MVX-3 group. The average secretion slightly increased and reached a similar level in both groups at Day 21 (702 ng/24 h/capsule in the MVX-2 + WT group, and 719 ng/24 h/capsule in the MVX-2 + MVX-3 group). Myo-P devices loaded with 1 M of MVX-3 cells produced an average of 3395 ng/24 h/capsule of anti-CTLA4 antibody at Day 1 and maintained their secretion to reach an average of 2980 ng/24 h/capsule at Day 21. Myo-P devices loaded with half the MVX-3 cells (0.5 M) secreted 1264 ng/24 h/capsule at Day 1 and increased their secretion until reaching a plateau at Day 4 to reach an average production of anti-CTLA4 antibody of 2184 ng/24 h/capsule at Day 21. Myo-P devices loaded with 0.5 M of MVX-3 + 0.5 M of MVX-2 cells produced an average of 1382 ng/24 h/capsule of anti-CTLA4 antibody at Day 1 and 821 ng/24 h/capsule at Day 21. The same trend was observed in Myo-P devices loaded with 0.5 M of MVX-3 + 0.5 M of WT cells, with an anti-CTLA4 antibody production of 1637 ng/24 h/capsule at Day 1 and 1045 ng/24 h/capsule at Day 21.

In a second experiment, Myo-P devices loaded with the same combinations of cell lines were implanted into C57/BL6 mice and kept for one week subcutaneously. A 2-h *in vitro* release was performed before

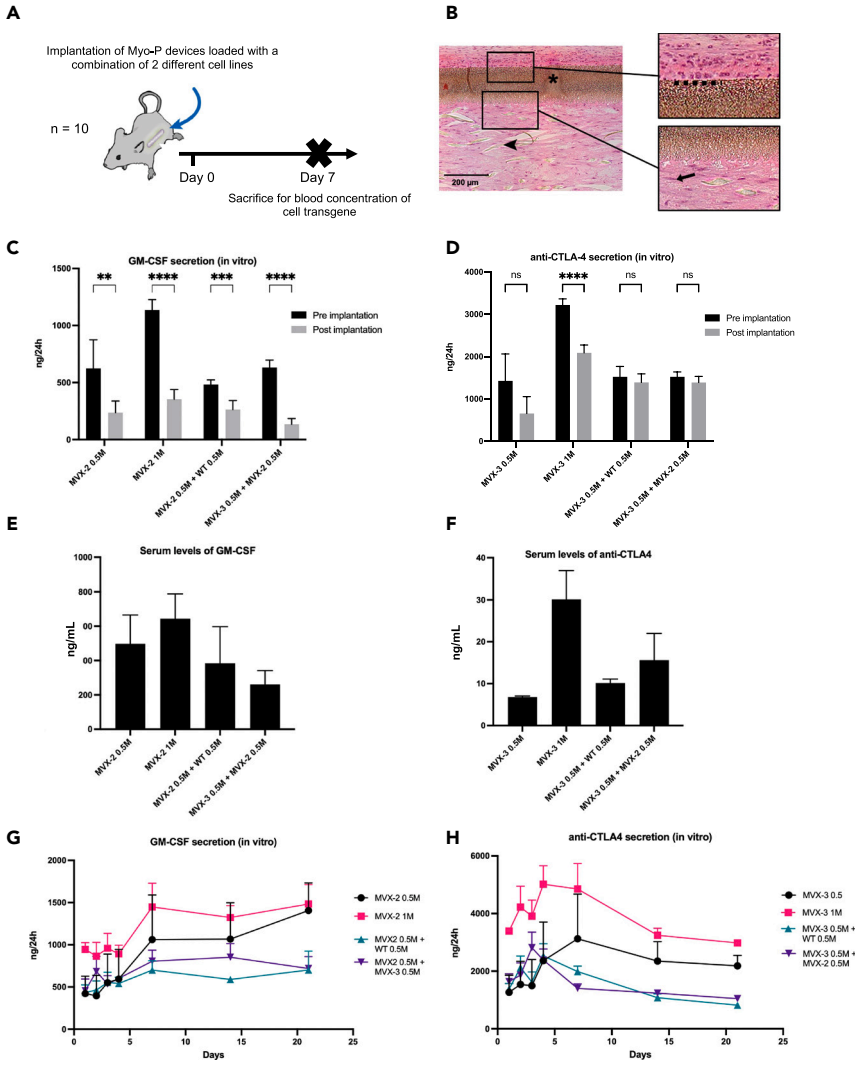

Figure 5. Versatility of the Myo-P device

Wild type cells (WT), huGM-CSF-secreting cells (MVX-2) and anti-CTLA4 antibody secreting cells (MVX-3) were encapsulated either alone or in combination, at different concentrations in the Myo-P device.

(A) Scheme of the experimental procedure.

(B) Histological section of the Myo-P device (without reinforcement coil for imaging purpose) loaded with MVX-2 cells after one week implantation in the mouse subcutaneous tissue. H&E staining of the myoblast cells in the Myo-P device (arrow), as well as the external cells (dots). Asterisk depicts the semi-permeable membrane. Arrowhead points to the yarn that optimizes the spatial distribution and provides a physical support for adherent cells.

(C–F) Devices were subsequently implanted into C57/BL6 mice and kept for one week in the mice. A 24-h *in vitro* release was performed before implantation and after explantation to measure the huGM-CSF (C) and anti-CTLA4 antibody (D) secretion by ELISA. (E and F) Serum samples were collected from implanted mice to quantify huGM-CSF (E) and anti-CTLA4 antibody (F) levels by ELISA. (C–F) Each bar represents mean ± SD of n = 10 replicates.

(G and H) Devices were maintained in culture for 21 days and the expression of huGM-CSF (G) and anti-CTLA4 antibody (H) was quantified by ELISA over time. (G and H) Each dot represents mean ± SD of n = 5 replicates.

** means significant difference (t-test) and $p < 0.01$; *** means significant difference and $p < 0.001$; **** means significant difference and $p < 0.0001$. ns means non-significant difference.

implantation and immediately after explantation to measure the huGM-CSF, and anti-CTLA4 antibody secretion by ELISA. After explantation, GM-CSF secretion substantially decreased in all groups (Figure 5B). Myo-P devices loaded with 1M of MVX-2 cells produced on average 1136 ng/24 h/capsule of GM-CSF at baseline and 236 ng/24 h/capsule after explantation. Similarly, Myo-P devices loaded with 0.5 M of MVX-2 cells produced on average 624 ng/24 h/capsule of GM-CSF at baseline and 236 ng/24 h/capsule

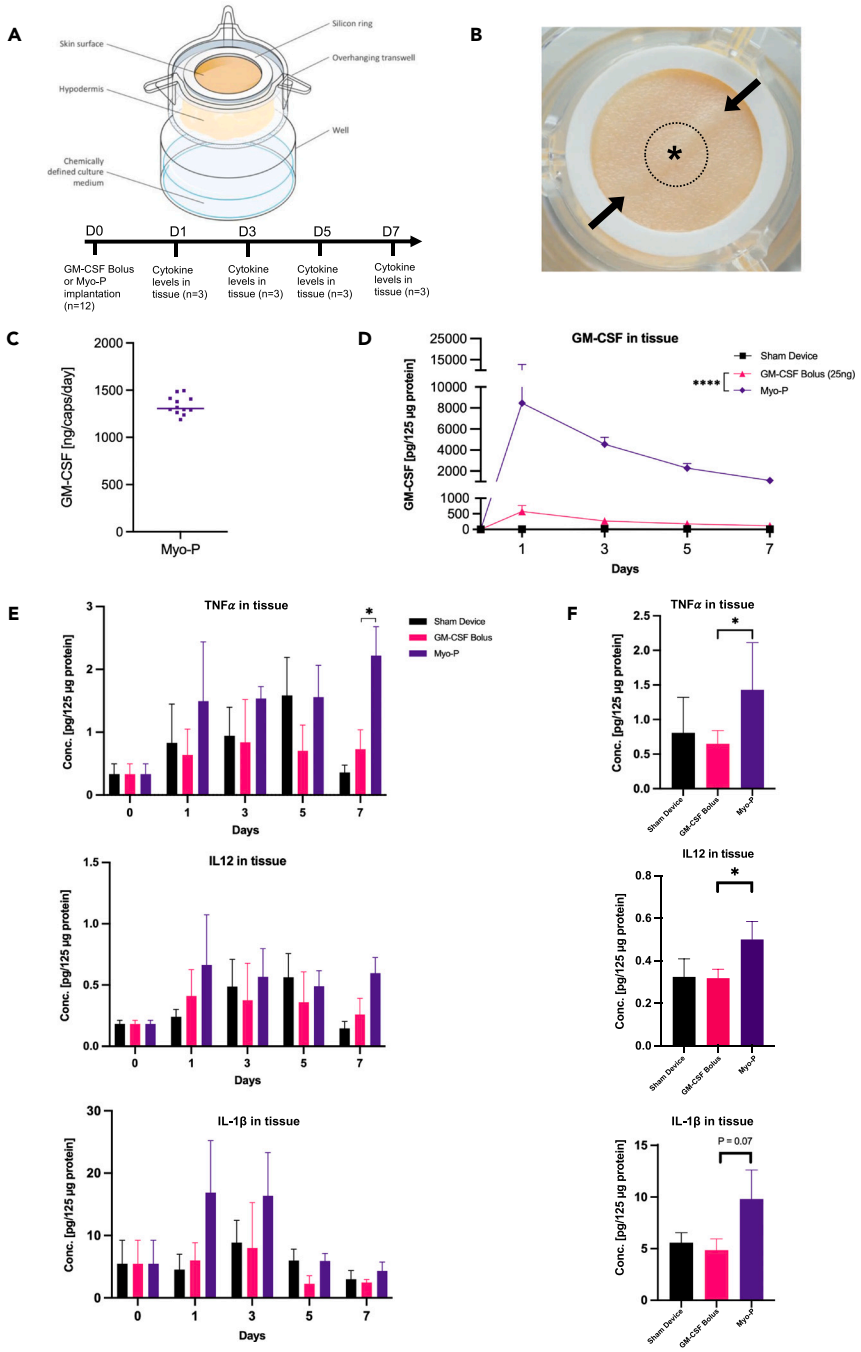

Figure 6. Local pharmacokinetic and pharmacodynamic profile of Myo-P device loaded with huGM-CSF-secreting cells (MVX-2) implanted in an *ex vivo* human skin model

(A) Scheme of the experimental procedure. Myo-P device (empty or with MVX-2 cells) or bolus huGM-CSF (25 ng) was subcutaneously implanted or injected, respectively, in HypoSkin models. Punch biopsies were sampled at Day 1, 3, 5 and 7 after implantation.

(B) Top view of the HypoSkin model. The arrows are pointing to the distal and proximal ends of the Myo-P device. Asterisk depicts the location of the bolus injection of GM-CSF. The dotted circle depicts the location punch biopsy.

(C) Prior to implantation, a 24-h release was performed to measure the huGM-CSF secretion by ELISA.

(D) Devices were subsequently implanted into HypoSkin models and kept for up to one week, according to the scheme of experiment. Tissue samples were collected to quantify huGM-CSF levels by ELISA. Each dot represents mean ± SD of n = 3 replicates.

Figure 6. *Continued*

(E and F) Proinflammatory cytokines were also quantified by multiplex from tissue samples. (E) Proinflammatory cytokines levels at each time points. (F) Mean levels of proinflammatory cytokines over 7 days. (E and F) Each bar represents mean ± SD of n = 3 replicates. Statistical significance of AUC was assessed by two-way analysis of variance followed by Tukey's multiple comparison test. **** means significant difference and $p < 0.0001$. For comparison between 2 groups, statistical significance was assessed by Student's *t* test. * means significant difference and $p < 0.05$.

after explantation. The same trend was observed in Myo-P devices loaded with two different cell lines: the GM-CSF-secreting capabilities decreased from an average of 483 ng/24 h/capsule at baseline to 263 ng/24 h/capsule post-explantation in Myo-P devices loaded with 0.5 M of MVX-2 + 0.5 M of WT cells, and from an average of 631 ng/24 h/capsule to 134 ng/24 h/capsule in Myo-P devices loaded with 0.5 M of MVX-2 + 0.5 M of MVX-3 cells. While a similar trend was observed for the anti-CTLA4 antibody-secreting capabilities in Myo-P devices loaded with MVX-3 cells alone, it was not observed in Myo-P devices loaded with two different cell lines (Figure 5C). Myo-P devices loaded with 1 M of MVX-3 cells produced an average of 3220 ng/24 h/capsule at baseline and 2089 ng/24 h/capsule post-explantation, and Myo-P devices loaded with 0.5 M of MVX-3 cells produced 1427 ng/24 h/capsule at baseline and 657 ng/24 h/capsule after explantation. In Myo-P devices loaded with two different cell lines; the anti-CTLA4 antibody-secreting capabilities did not decrease significantly. Serum from implanted mice was also collected at Day 7 post implantation, for both GM-CSF and anti-CTLA4 antibody quantification by ELISA. Serum level of GM-CSF reached an average of 643 and 497 pg/mL in mice implanted with 1M and 0.5 M of MVX-2 cells, respectively, and an average of 384 and 261 pg/mL in in mice implanted with 0.5 M of MVX-2 cells +0.5 M of WT cells and 0.5 M of MVX-2 cells +0.5 M of MVX-3 cells, respectively (Figure 5D). Serum level of anti-CTLA4 antibody reached an average of 30.1 and 6.8 ng/mL in mice implanted with 1 M and 0.5 M of MVX3 cells, respectively, and an average of 10.1 and 15.6 ng/mL in in mice implanted with 0.5 M of MVX-3 + 0.5 M of WT cells and 0.5 M of MVX-3 + 0.5 M of MVX-2 cells, respectively (Figure 5E). Overall secretion levels tend to indicate that confluence is reached with 1 M loaded cells. Secretion and serum levels are consistently reflecting the number of cells loaded in Myo-P devices, and the results support the absence of cell-cell interaction that would impair the secretion capably in the Myo-P device.

In a third experiment, Myo-P devices built without reinforcement coil for imaging purposes were loaded with 1 M MVX-2 cells. After one week in the mouse subcutaneous tissue, many viable myoblastic cells are observed in the inner chamber (Figure 5H), suggesting that the Myo-P device effectively protects its cargo against external cells. Myo-P biocompatibility was characterized according to the EN ISO 10993.[30] The results are outlined in Table S3. The biological evaluation of all data, including information gathered from published scientific literature on top of the favorable biocompatibility results, supports the acceptable biocompatibility profile of the Myo-P device for use as intended in adults. The reversibility of the intervention along with the fact that the encapsulated cells never enter into direct contact with the host strongly mitigate the risk of inflammation at implantation site.

Potential therapeutic application of Myo-P2 as adjuvant

Myo-P devices loaded with huGM-CSF-secreting (MVX-2) cells were subcutaneously implanted in an *ex vivo* human skin model for seven days (Figures 6A and 6B). MVX-2 cells were selected because they are a nontumorigenic, human myoblast cell line which displays contact inhibition, are amenable to genetic modification, and have been characterized for clinical use.[33] The huGM-CSF, as well as a selected panel of proinflammatory cytokine concentrations, was measured in adjacent tissue at days 1, 3, 5, and 7 to characterize both the pharmacokinetic and the pharmacodynamic of the intervention. A 25-ng bolus injection of recombinant huGM-CSF was used as comparator. Such dose was selected to match the acceptable range defined in the target product profile of MVX-ONCO-1.[24] AUC was 27445 a.u. (SD 8541, 95% CI 10704 to 44185) in the Myo-P group, and 1876 au (SD 417.2, 95% CI 1059 to 2694) in the bolus injection group (Figure 6D). The average tissue concentration over seven days of three pro-inflammatory cytokines previously described as related to GM-CSF, namely TNF alpha, IL-1 Beta and IL-12,[36,37] was significantly higher in the Myo-P group than in the bolus injection group (Figures 6E and 6F). The results suggest that the Myo-P device enables the production of immunomodulatory cytokines, such as GM-CSF, by encapsulated cells for up to seven days in human skin. The extended production is consequently reflected by a distinctive prolonged, local pharmacodynamic effect compared to the bolus, as demonstrated by the tissue concentration of three pro-inflammatory cytokines in specific response to GM-CSF.

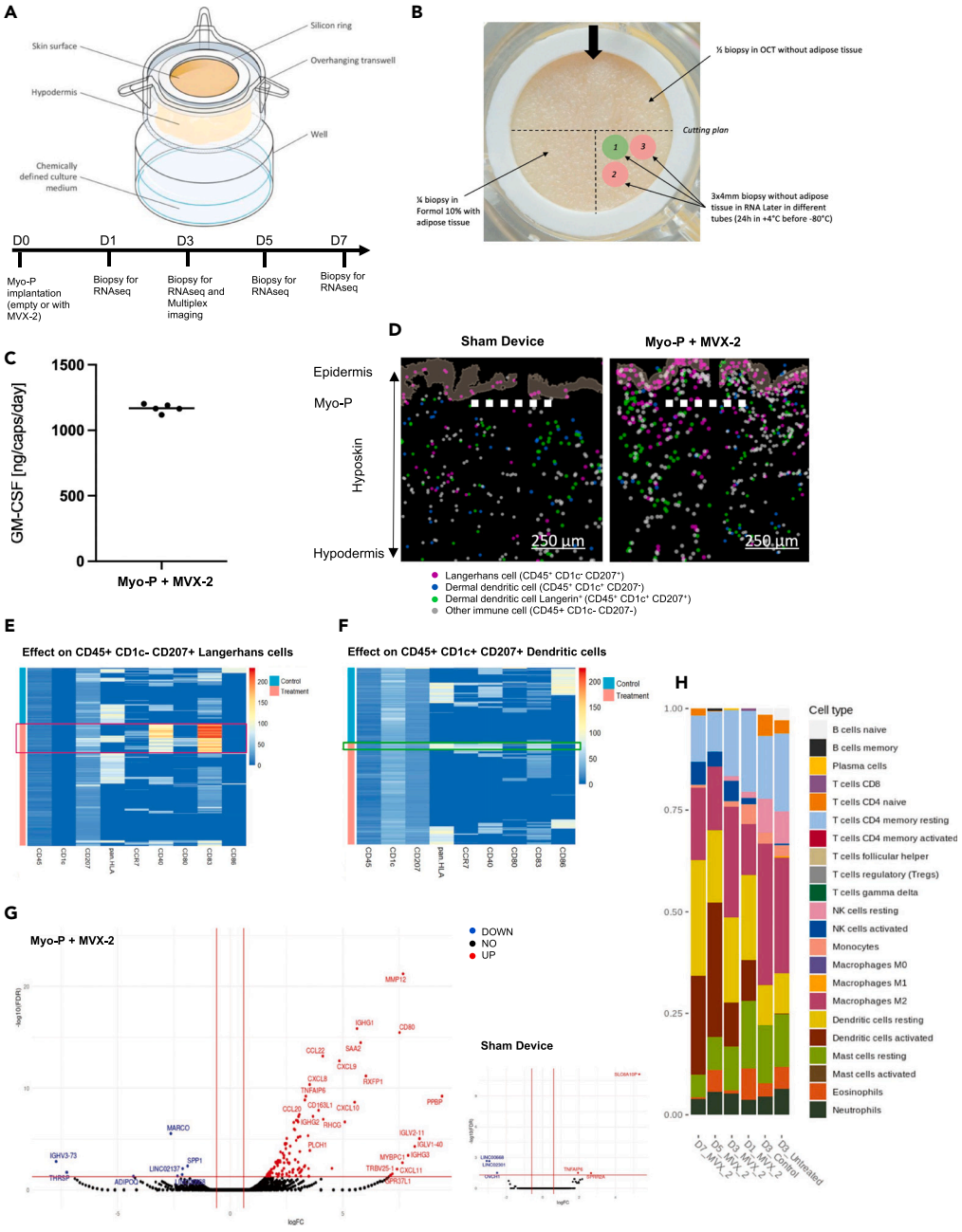

Figure 7. Demonstration of Antigen-Presenting Cell (APC) mobilization and activation by the Myo-P device loaded with huGM-CSF-secreting cells (MVX-2) in an *ex vivo* human skin model

(A) Scheme of the experimental procedure. Myo-P devices (empty or with huGM-CSF-secreting cells) were subcutaneously implanted in Hyposkin models. Punch biopsies were sampled at Day 1, 3, 5 and 7 after implantation (only at Day 3 for the empty Myo-P).

(B) Top view of the HypoSkin model. The arrow is pointing to the Myo-P device.

(C) Prior to implantation, a 24-h release was performed to measure the huGM-CSF secretion by ELISA.

(D) Digital maps showing the spatial organization of APCs at the implantation site at Day 3. The white dotted line indicates the location of the Myo-P/sham device. Populations of Langerin^{+} dermal DCs and Langerhans cells were found closer to the site of the Myo-P2 condition.

(E) Heatmap of implantation site at Day 3 showing an induction of a population of Langerhans cells that express CD45^{+} CD1c- CD207+ pan-HLA+ CCR7+ CD40high CD80^{+} CD83high CD86^{-}only in the GM-CSF treated condition.

Figure 7. *Continued*

(F) Heatmap of implantation site at Day 3 showing an induction of a population of Langerin+ dermal dendritic cells that express CD45^{+} CD1c+ CD207+ pan-HLAmed CCR7med CD40med CD80^{-} CD83med CD86^{-}only in the MVX-2 treated condition.

(G) Volcano plot representing the statistically significant DEGs at Day 3. Scatterplots showed the -log 10 of the false discovery rate (FDR) versus the log of magnitude of change (fold change). Upregulated genes are in blue, and downregulated genes are in red.

(H) Immune cell type abundance at Day 1, 3, 5 and 7 in the GM-CSF treated condition (labeled MVX-2), and Day 3 in the control.

See also Figures S1, S2, and Tables S4–S6.

In a different experiment conducted in the same model, we explored the Antigen-Presenting Cell (APC) mobilization and activation by the Myo-P2 device. We used Multiplex ANnotated Imaging System (MANTIS)[38] and bulk RNA sequencing (Figures 7A and 7B) to characterize the pharmacodynamic signature of the intervention over 7 days. Antigen-Presenting Cell (APC) populations, including Langerhin+ dermal DCs and Langerhans cells were found closer to the site of the Myo-P2 device than the sham device at Day 3 (Figure 7D). Two APC populations exhibited a hyper-activated phenotype only in Myo-P2 treated condition, with Langerhans cells CD45^{+} CD1c- CD207+ CD80^{+} CD40high CD83high (Figure 7E) and dermal Langerin+ dendritic cells CD45^{+} CD1c+ CD207+ CD40med CD83med CCR7med pan-HLAmed (Figure 7F). The major effect of the Myo-P2 on gene expression over time was observed from Day 1 to Day 3; 119 genes were differentially expressed in the Myo-P2 versus only 6 in the sham device group (Figure 7G). Volcano plots representing the statistically significant DEGs at Day 1, 5 and 7 are described in Figure S1. These genes are mainly related to immune cell chemotaxis, antigen presentation and immunoglobulin production (Tables S4–S6).[39,40] An increasing amount of activated dendritic cells was observed in the Myo-P2 group over time (Figure 7H) compared to the sham device group. Overall, when evaluating the differences in the immune profiling and spatial distribution of immune cells in human skin tissue, the results highlight a clear increase, mobilization and activation of 2 populations of skin APCs in the Myo-P2 treated condition compared to the sham device.

DISCUSSION

The delivery of therapeutic proteins by genetically engineered, encapsulated cells could emerge as an alternative to repeated bolus administrations, and potentially improve chronic disease management.[2,41] Here, we have developed the Myo-P device; an implant for the delivery of therapeutic proteins, that is fully biocompatible, scalable, and easy to administer, retrieve or replace. We were able to demonstrate the improved features of the Myo-P device compared to its predecessor, the GEN-1 device, toward mechanical and functional performance. The matrix incorporated in the Myo-P allows for suspension cells to grow and survive with optimized spatial distribution, and adherent cells such as myoblasts, to attach and fuse together to form myotubes.[15,19] Both the *in vitro* and *in vivo* secretion capacity are improved with the Myo-P device compared to the GEN-1 device; with the same secreting cell line at the same concentration, the *in vitro* secretion of huGM-CSF was 1.5 times higher with the Myo-P than with the GEN-1 device at baseline, and the tissue concentration of huGM-CSF was 4 times higher and the serum concentration was 17 times higher in the Myo-P than in the GEN-1 device seven days post implantation. The built-in polypropylene thread embedded in the proximal glue point of the retrieval tube provides the user with a ready-to-use device, instead of requiring the user to attach a suture to the hook prior to implantation, as was the case with the GEN-1 device. The Myo-P device administration procedure in humans remains the same as the GEN-1 device administration procedure, which is straightforward for physicians, and not burdensome for patients.[26]

Both suspension and adherent cells were loaded into the Myo-P device, cultured *in vitro* and implanted in mice. The results demonstrated that both types of cell line survive well in the Myo-P device *in vitro* and *in vivo*. Different cell lines secreting different proteins can also be combined in the Myo-P device, and the secretion capability of the transgene of interest can be adjusted by adapting the proportion of cells in the device. Several devices can easily be co-administered, which makes the technology scalable *in vivo*. Recent investigations have shown that tumor-adjacent administration of different encapsulated proinflammatory cytokines demonstrated predictable dose modulation with spatial and temporal control and enabled cancer immunotherapy without systemic toxicities.[42] Combining different cytokine-secreting cells in the Myo-P device could lead to effective cytokine therapy, without requiring high-dose infusions that can result in anti-drug antibodies and/or systemic side effects that limit long-term benefits.[43] This technology

could also improve the synergy between proteins with suboptimal systemic delivery such as GM-CSF and anti-CTLA4 antibody for anti-cancer therapy.[44,45] In a proof-of-concept experiment for the long-term delivery of therapeutic protein, we demonstrated that Myo-P-encapsulated myoblast cells maintain their secretion capabilities and produce measurable levels in the blood for more than 9 months in a murine model. We also demonstrated that the Myo-P device effectively protects its cargo against external cells. It is interesting to speculate that the function of the secreted molecule by the encapsulated cells matters and may impact the scope and the duration of the intended application: while the delivery of molecules with a distant target can be extended to several months, delivery of inflammatory molecules should be limited to several days. Indeed, both the inward diffusion of nutrients, trophic factors and oxygen, essential for the survival of encapsulated cells, and the outward diffusion of the therapeutic protein are likely to be impaired by the influx and clustering of immune cells around the device.[46] In both cases, further investigations in disease models are required.

A major logistical aspect to consider during the development of a clinically translatable implant for the delivery of therapeutic protein is its ability to endure freezing, storage in liquid nitrogen, and thawing.[47] To assess such features, Myo-P devices were loaded with MVX-2 cells, subsequently frozen and stored in liquid nitrogen. Devices were then thawed and cultured *in vitro*. Their secretion capability was comparable to the ones that remained in culture after loading. The variability is inherent to the biologic nature of the ELISA assay and remains within the acceptable tolerance of suitable analytical methods.[48]

We also investigated the potential of Myo-P devices loaded with GM-CSF secreting cells to mobilize and activate APCs in a human skin model. GM-CSF-based vaccines have been shown to elicit potent antitumor and antiviral immune responses in preclinical experiments, as well as in some clinical studies,[49–54] and many concluded that both the delivery and the dose matters.[55,56] While sustained, low doses of GM-CSF at vaccination sites might increase the vaccine-induced immune response, systemic administration of high doses (100 μg–500 μg) of GM-CSF might mediate an immune suppression by activating and expanding myeloid suppressor cells.[57–60] First, we investigated the effect of sustained exposure to huGM-CSF in models implanted with Myo-P2 devices over seven days, compared with a bolus injection of recombinant huGM-CSF. In this experiment, we observed a higher exposure to huGM-CSF over seven days along with a higher expression of proinflammatory cytokines in response to huGM-CSF in the Myo-P2 device group compared to the bolus.[36,37,61] Finally, we characterized the immune cell mobilization and activation by Myo-P2 devices. The three main skin APC subtypes were detected in both the treated and the control conditions (Langerhans cells, Langerin+ Dermal dendritic cells and dermal dendritic cells). Both the Langerhans cells and Langerin+ dermal dendritic cell populations exhibited a hyper-activated phenotype in the Myo-P2 condition. These two populations express most of required co-stimulatory molecules to trigger naive T cell activation.[62,63] In addition, the population of Langerin+ dermal dendritic cells was found closer to the site of capsule implantation and expressed CCR7, which is a major chemokine receptor involved in the homing to the draining lymph node.[64,65] Based on this preliminary analysis, it is interesting to speculate that the latter population could be the one that would uptake the antigens and migrate to trigger an adaptive immune response in the draining lymph node. Further investigations would be required to affirm such speculation. To further characterize the local pharmacodynamic effects, the gene expression was also analyzed by bulk RNA sequencing. From Day 1 to Day 3, the Myo-P2 device had a clear impact on gene expression, with 119 DEGs versus only 6 in the sham device group. In the treated condition, upregulated genes were related to immune cell chemotaxis, antigen presentation, immunoglobulin production, other immune functions, and tissue remodeling.[66] Two trends were identified. On the one hand, upregulated gene expressions were related to adaptive immunity, in particular to attraction and migration of T-cells and dendritic cells: at all time-points, CCL17, which is involved in trafficking and activation of mature T-cells, was highly overexpressed.[67,68] DEGs suggested the involvement of leukocytes, particularly on Day 3. On the other hand, gene expressions which were downregulated were linked to host defense against pathogens, inhibition of the T cell response and mast cells, suggesting a downregulation of innate immunity (Tables S4–S6).[69] Other processes were detected in response to Myo-P2s: cell division (Day 1), extracellular matrix remodeling (with high upregulation of MMP12 over seven days), cell metabolism, and skin homeostasis (Days 5 and 7). These results suggest huGM-CSF released by Myo-P2 devices in HypoSkin for seven days activates at least two populations of antigen-presenting cells over time, and stimulates skin-resident immune cells, with T cell, dendritic cells and neutrophil attraction and migration. It bolsters the exploration of Myo-P2 devices as adjuvant in cancer immunization schemes. Overall, we believe that our technology may contribute to cell therapies in different indications, and potentially improve the management of chronic diseases.

Limitations of the study

There are several limitations to studies presented in this report. First, systemic protein delivery was assessed with encapsulated human cells secreting human proteins in a murine model; the xenogeneic nature of the encapsulated cells may have triggered an adaptive immune response altering the blood level of delivered protein, which may not accurately reflect an allogeneic setting. Second, for the *in vivo* work, a 1-week implantation period was defined. Here again, it is partly due to the xenogeneic nature of the intervention as the component of the immune response directed against xenogeneic antigens is typically very strong. In all GM-CSF/anti-CTLA-4 related experiment, we defined the duration of 1-week because the aim is immunization. Additional *in vivo* work should be performed in an appropriate model to show the *in vivo* function of the technology for longer than 100-day, which is typically considered a threshold for assessing mitigation strategies against chronic rejection. Third, the key observations related to the potential therapeutic application of the Myo-P2 as adjuvant in cancer immunization strategies were performed in an *ex vivo* human skin model. Such model holds the features and functionalities of *in vivo* human skin, with all skin and immune cells, and generate predictive human data. It is suitable for local pharmacological characterization; however, it may not accurately reflect a fully vascularized human skin. Finally, it was not possible to explore comparative multiplexed imaging between the Myo-P2 and the bolus injection of GM-CSF and, as such, the sham device was used as control: while it is easy to locate devices, the precise location of the bolus is difficult to determine in 3D and less reliable to assess cell mobilization in that particular case. The latter limitation is mitigated by the similar pharmacodynamic profile between the bolus injection and the sham device (Figures 6E and 6F). Nevertheless, despite these limitations we believe these data provide a ground for further exploring this technology in therapeutic models.

STAR★METHODS

Detailed methods are provided in the online version of this paper and include the following:

- KEY RESOURCES TABLE
- RESOURCE AVAILABILITY
  - Lead contact
  - Materials availability
  - Data and code availability
- EXPERIMENTAL MODEL AND STUDY PARTICIPANT DETAILS
  - Animals
  - Ex vivo human skin model
  - Media and reagents
- METHOD DETAILS
  - Device manufacturing
  - Mechanical characterization
  - Cell encapsulation
  - Freezing and thawing of loaded Myo-P capsules
  - Implantation of capsules in mice
  - Implantation in an ex vivo human skin model
  - Tissue preparation
  - Protein quantification
  - Multiplexed imaging
  - Skin bulk RNA sequencing
- QUANTIFICATION AND STATISTICAL ANALYSIS
- ADDITIONAL RESOURCES

SUPPLEMENTAL INFORMATION

Supplemental information can be found online at https://doi.org/10.1016/j.isci.2023.107372.

ACKNOWLEDGMENTS

The authors would also like to thank Genoskin for their human skin model, and Scicomvisuals for the preparation of the graphical abstract and the video S1. This project was supported by the Private Foundation of the Geneva University Hospitals, Fondation Coromandel, Philanthropy Settlement Foundation and

Maxivax SA. It also received funding from the European Union's Horizon 2020 research and innovation program under grant agreement No 880194.

AUTHOR CONTRIBUTIONS

Conceptualization: J.G., A.L., and N.M.; Methodology: J.G., A.L., and N.M.; Formal analysis: J.G., R.V., E.C., N.G., A.E., and N.M.; Investigation: J.G., R.V., E.C., M.U., O.V.R., V.S., F.C., N.G., A.E., and A.L; Resources: J.G., A.L., and N.M.; Data Curation: J.G., N.G., and M.U.; Writing – Original Draft: J.G.; Writing – Review and Editing: J.G., R.V., E.C., N.G., A.E., A.L., and N.M.; Visualization: J.G., R.V., E.C., M.U., N.G., and A.E.; Supervision: J.G. and N.M.; Project administration: J.G. and N.M.; Funding acquisition: J.G., A.L., and N.M.

DECLARATION OF INTERESTS

N.M. is founder and stockholder of MaxiVAX SA, one of the sponsors of this work. J.G., E.C., and A.E. are employees of MaxiVAX SA. A.L. is a former employee of MaxiVAX SA. A.L., J.G., and N.M. are inventors in a patent related to this work. MaxiVAX SA is a Geneva-based biotech company involved in cell encapsulation technology.

INCLUSION AND DIVERSITY

We support inclusive, diverse, and equitable conduct of research.

Received: May 22, 2023
Revised: June 12, 2023
Accepted: July 10, 2023
Published: July 13, 2023

REFERENCES

1. Santos-Vizcaino, E., Orive, G., Pedraz, J.L., and Hernandez, R.M. (2020). Clinical applications of cell encapsulation technology. In Methods in Molecular Biology (Humana Press Inc), pp. 473–491. https://doi.org/10.1007/978-1-0716-0215-7_32.

2. Farina, M., Alexander, J.F., Thekkedath, U., Ferrari, M., and Grattoni, A. (2019). Cell encapsulation: overcoming barriers in cell transplantation in diabetes and beyond. Adv. Drug Deliv. Rev. *139*, 92–115. https://doi.org/10.1016/j.addr.2018.04.018.

3. Orive, G., Santos, E., Poncelet, D., Hernández, R.M., Pedraz, J.L., Wahlberg, L.U., de Vos, P., and Emerich, D. (2015). Cell encapsulation: technical and clinical advances. Trends Pharmacol. Sci. *36*, 537–546. https://doi.org/10.1016/j.tips.2015.05.003.

4. Vila, ' A, Sanchez, A., Tobıo, M., Calvo, P., and Alonso, M.J. (2002). Design of biodegradable particles for protein delivery. J. Control Release *78*, 15–24.

5. Désiré, L., Mysiakine, E., Bonnafous, D., Couvreur, P., Sagodira, S., Breton, P., and Fattal, E. (2006). Sustained delivery of growth factors from methylidene malonate 2.1.2-based polymers. Biomaterials *27*, 2609–2620. https://doi.org/10.1016/j.biomaterials.2005.11.041.

6. Garbayo, E., Ansorena, E., Lana, H., Carmona-Abellan, M.D.M., Marcilla, I., Lanciego, J.L., Luquin, M.R., Blanco-Prieto, M.J., and Blanco-Prieto, M.J. (2016). Brain delivery of microencapsulated GDNF induces functional and structural recovery in parkinsonian monkeys. Biomaterials *110*, 11–23. https://doi.org/10.1016/j.biomaterials.2016.09.015.

7. Chua, C.Y.X., Ho, J., Demaria, S., Ferrari, M., and Grattoni, A. (2020). Emerging technologies for local cancer treatment. Adv. Ther. *3*, 2000027. https://doi.org/10.1002/adtp.202000027.

8. Orive, G., Santos-Vizcaino, E., Pedraz, J.L., Hernandez, R.M., Vela Ramirez, J.E., Dolatshahi-Pirouz, A., Khademhosseini, A., Peppas, N.A., and Emerich, D.F. (2019). 3D cell-laden polymers to release bioactive products in the eye. Prog. Retin. Eye Res. *68*, 67–82. https://doi.org/10.1016/j.preteyeres.2018.10.002.

9. Grogg, J., Charrier, E., Vernet, R., Urwyler, M., Von Rohr, O., Saingier, V., Courtout, F., Lathuiliere, A., Engel, A., and Mach, N. (2023). Sustained delivery of low-dose anti-CTLA-4 by genetically engineered encapsulated cells to the tumor microenvironment drives tumor response and prolongs survival in a colorectal cancer model. Cancer Res. *83*, 2721. https://doi.org/10.1158/1538-7445.AM2023-2721.

10. Lopez-Mendez, T.B., Santos-Vizcaino, E., Pedraz, J.L., Hernandez, R.M., and Orive, G. (2021). Cell microencapsulation technologies for sustained drug delivery: clinical trials and companies. Drug Discov. Today *26*, 852–861. https://doi.org/10.1016/j.drudis.2020.11.019.

11. Bhujbal, S.v., de Haan, B., Niclou, S.P., and de Vos, P. (2014). A novel multilayer immunoisolating encapsulation system overcoming protrusion of cells. Sci. Rep. *4*, 6856. https://doi.org/10.1038/srep06856.

12. Orive, G., Santos, E., Pedraz, J.L., and Hernández, R.M. (2014). Application of cell encapsulation for controlled delivery of biological therapeutics. Adv. Drug Deliv. Rev. *67–68*, 3–14. https://doi.org/10.1016/j.addr.2013.07.009.

13. Li, M., Wang, L., Wei, Y., Wang, W., Liu, Z., Zuo, A., Liu, W., Tian, J., and Wang, H. (2022). Macroencapsulation devices for cell therapy. Engineering *16*, 53–70. https://doi.org/10.1016/j.eng.2021.10.021.

14. Song, S., and Roy, S. (2016). Progress and challenges in macroencapsulation approaches for type 1 diabetes (T1D) treatment: cells, biomaterials, and devices. Biotechnol. Bioeng. *113*, 1381–1402. https://doi.org/10.1002/bit.25895.

15. Lathuilière, A., Cosson, S., Lutolf, M.P., Schneider, B.L., and Aebischer, P. (2014). A high-capacity cell macroencapsulation system supporting the long-term survival of genetically engineered allogeneic cells. Biomaterials *35*, 779–791. https://doi.org/10.1016/j.biomaterials.2013.09.071.

16. Lee, D.Y., Park, S.J., Lee, S., Nam, J.H., and Byun, Y. (2007). Highly poly(ethylene) glycolylated islets improve long-term islet allograft survival without immunosuppressive medication. Tissue Eng. *13*, 2133–2141. https://doi.org/10.1089/TEN.2006.0009.

17. Vériter, S., Mergen, J., Goebbels, R.M., Aouassar, N., Grégoire, C., Jordan, B., Levêque, P., Gallez, B., Gianello, P., and Dufrane, D. (2010). In vivo selection of biocompatible alginates for islet encapsulation and subcutaneous transplantation. Tissue Eng. Part A *16*, 1503–1513. https://doi.org/10.1089/TEN.TEA.2009.0286.

18. Lathuilière, A., Laversenne, V., Astolfo, A., Kopetzki, E., Jacobsen, H., Stampanoni, M., Bohrmann, B., Schneider, B.L., and Aebischer, P. (2016). A subcutaneous cellular implant for passive immunization against amyloid-β reduces brain amyloid and tau pathologies. Brain *139*, 1587–1604. https://doi.org/10.1093/brain/aww036.

19. Bose, S., Volpatti, L.R., Thiono, D., Yesilyurt, V., McGladrigan, C., Tang, Y., Facklam, A., Wang, A., Jhunjhunwala, S., Veiseh, O., et al. (2020). A retrievable implant for the long-term encapsulation and survival of therapeutic xenogeneic cells. Nat. Biomed. Eng. *4*, 814–826. https://doi.org/10.1038/s41551-020-0538-5.

20. Chew, E.Y., Clemons, T.E., Jaffe, G.J., Johnson, C.A., Farsiu, S., Lad, E.M., Guymer, R., Rosenfeld, P., Hubschman, J.P., Constable, I., et al. (2019). Effect of ciliary neurotrophic factor on retinal neurodegeneration in patients with macular telangiectasia type 2: a randomized clinical trial. Ophthalmology *126*, 540–549. https://doi.org/10.1016/j.ophtha.2018.09.041.

21. Farina, M., Ballerini, A., Fraga, D.W., Nicolov, E., Hogan, M., Demarchi, D., Scaglione, F., Sabek, O.M., Horner, P., Thekkedath, U., et al. (2017). 3D printed vascularized device for subcutaneous transplantation of human islets. Biotechnol. J. *12*, 1700169. https://doi.org/10.1002/biot.201700169.

22. Schwenter, F., Zarei, S., Luy, P., Padrun, V., Bouche, N., Lee, J.S., Mulligan, R.C., Morel, P., and MacH, N. (2011). Cell encapsulation technology as a novel strategy for human anti-tumor immunotherapy. Cancer Gene Ther. *18*, 553–562. https://doi.org/10.1038/cgt.2011.22.

23. Lathuilière, A., Mach, N., and Schneider, B.L. (2015). Encapsulated cellular implants for recombinant protein delivery and therapeutic modulation of the immune system. Int. J. Mol. Sci. *16*, 10578–10600. https://doi.org/10.3390/ijms160510578.

24. Mach, N., Vernet, R., Belkouch, M.-C., Luy, P., Ancrenaz, V., Teta, P., Blazek, N., Grandjean, N., Wasem, J., Grogg, J., et al. (2016). MVX-ONCO-1 phase 1 final results of the first personalized cell-based immunotherapy using cell encapsulation technology. Ann. Oncol. *27*, vi362. https://doi.org/10.1093/annonc/mdw378.12.

25. Grogg, J., Lathuilière, A., and Mach, N. (2021). Implantable Capsule. World Intellectual Property Organisation.

26. Fernandez, E., Vernet, R., Charrier, E., Migliorini, D., Joerger, M., Belkouch, M.-C., Urwyler, M., Rohr, O., Saingier, V., Ancrenaz, V., et al. (2021). MVX-ONCO-1 in advanced refractory cancers: Safety, feasibility, and preliminary efficacy results from all HNSCC patients treated in two ongoing clinical trials. J. Clin. Oncol. *39*, e18005.

27. Nguyen, P.T., Asarias, J.R., and Pierce, L.M. (2012). Influence of a new monofilament polyester mesh on inflammation and matrix remodeling. J. Invest. Surg. *25*, 330–339. https://doi.org/10.3109/08941939.2011.639848.

28. Yamasaki, L.C., de Vito Moraes, A.G., Barros, M., Lewis, S., Francci, C., Stansbury, J.W., and Pfeifer, C.S. (2013). Polymerization development of "low-shrink" resin composites: reaction kinetics, polymerization stress and quality of network. Dent. Mater. *29*, e169–e179. https://doi.org/10.1016/j.dental.2013.04.021.

29. Wang, L., Chen, D., Jiang, K., and Shen, G. (2017). New insights and perspectives into biological materials for flexible electronics. Chem. Soc. Rev. *46*, 6764–6815. https://doi.org/10.1039/C7CS00278E.

30. FDA (2020). Biological Evaluation of Medical Devices-Part 1: Evaluation and Testing within a Risk Management Process.

31. Tan, F., and Al-Rubeai, M. (2019). Customizable implant-specific and tissue-specific extracellular matrix protein coatings fabricated using atmospheric plasma. Front. Bioeng. Biotechnol. *7*, 247. https://doi.org/10.3389/fbioe.2019.00247.

32. Lutolf, M.P., and Hubbell, J.A. (2005). Synthetic biomaterials as instructive extracellular microenvironments for morphogenesis in tissue engineering. Nat. Biotechnol. *23*, 47–55. https://doi.org/10.1038/nbt1055.

33. Lathuiliere, A., Vernet, R., Charrier, E., Urwyler, M., von Rohr, O., Belkouch, M.C., Saingier, V., Bouvarel, T., Guillarme, D., Engel, A., et al. (2022). Immortalized human myoblast cell lines for the delivery of therapeutic proteins using encapsulated cell technology. Mol. Ther. Methods Clin. Dev. *26*, 441–458. https://doi.org/10.1016/j.omtm.2022.07.017.

34. Maugham, M.L., Thomas, P.B., Crisp, G.J., Philp, L.K., Shah, E.T., Herington, A.C., Chen, C., Gregory, L.S., Nelson, C.C., Seim, I., et al. (2017). Insights from engraftable immunodeficient mouse models of hyperinsulinaemia. Sci. Rep. *7*, 491. https://doi.org/10.1038/s41598-017-00443-x.

35. Shinkai, Y., Rathbun, G., Lam, K.P., Oltz, E.M., Stewart, V., Mendelsohn, M., Charron, J., Datta, M., Young, F., and Stall, A.M. (1992). RAG-2-deficient mice lack mature lymphocytes owing to inability to initiate V(D)J rearrangement. Cell *68*, 855–867. https://doi.org/10.1016/0092-8674(92)90029-C.

36. Terao, I., Hashimoto, S., and Horie, T. (1993). Effect of GM-CSF on TNF-alpha and IL-1-beta production by alveolar macrophages and peripheral blood monocytes from patients with sarcoidosis. Int. Arch. Allergy Immunol. *102*, 242–248. https://doi.org/10.1159/000236532.

37. Lissoni, P., Fumagalli, E., Malugani, F., Ardizzoia, A., Bucovec, R., Tancini, G., and Gardani, G.S. (2001). Stimulation of IL-12 secretion by GM-CSF in advanced cancer patients. J. Biol. Regul. Homeost. Agents *15*, 163–165.

38. Scholaert, M., Houmadi, R., Martin, J., Nadine, S., Marie, T., Emilie, B., Lilian, B., Eric, M., Pascal, D., Manuelle, V., et al. (2023). 3-D deconvolution of human skin immune architecture with Multiplex Annotated Tissue Imaging System (MANTIS). Preprint at bioRxiv. https://doi.org/10.1101/2023.01.13.523748.

39. Carbon, S., Gene Ontology Consortium, Douglass, E., Good, B.M., Unni, D.R., Harris, N.L., Mungall, C.J., Basu, S., Chisholm, R.L., Dodson, R.J., Hartline, E., et al. (2021). The Gene Ontology resource: enriching a GOld mine. Nucleic Acids Res. *49*, D325–D334. https://doi.org/10.1093/nar/gkaa1113.

40. Ashburner, M., Ball, C.A., Blake, J.A., Botstein, D., Butler, H., Cherry, J.M., Davis, A.P., Dolinski, K., Dwight, S.S., Eppig, J.T., et al. (2000). Gene Ontology: tool for the unification of biology. Nat. Genet. *25*, 25–29. https://doi.org/10.1038/75556.

41. Bashor, C.J., Hilton, I.B., Bandukwala, H., Smith, D.M., and Veiseh, O. (2022). Engineering the next generation of cell-based therapeutics. Nat. Rev. Drug Discov. *21*, 655–675. https://doi.org/10.1038/s41573-022-00476-6.

42. Nash, A.M., Jarvis, M.I., Aghlara-Fotovat, S., Mukherjee, S., Hernandez, A., Hecht, A.D., Rios, P.D., Ghani, S., Joshi, I., Isa, D., et al. (2022). Clinically translatable cytokine delivery platform for eradication of intraperitoneal tumors. Sci. Adv. *8*, eabm1032.

43. Thom, A.K., Alexander, H.R., Andrich, M.P., Barker, W.C., Rosenberg, S.A., and Fraker, D.L. (1995). Cytokine levels and systemic toxicity in patients undergoing isolated limb perfusion with high-dose tumor necrosis factor, interferon gamma, and melphalan. J. Clin. Oncol. *13*, 264–273. https://doi.org/10.1200/JCO.1995.13.1.264.

44. Kwek, S.S., Kahn, J., Greaney, S.K., Lewis, J., Cha, E., Zhang, L., Weber, R.W., Leonard, L., Markovic, S.N., Fong, L., et al. (2016). GM-CSF and ipilimumab therapy in metastatic melanoma: clinical outcomes and immunologic responses. Oncoimmunology *5*, e1101204. https://doi.org/10.1080/2162402X.2015.1101204.

45. Duraiswamy, J., Kaluza, K.M., Freeman, G.J., and Coukos, G. (2013). Dual blockade of PD-1 and CTLA-4 combined with tumor vaccine effectively restores T-cell rejection function in tumors. Cancer Res. *73*, 3591–3603. https://doi.org/10.1158/0008-5472.CAN-12-4100.

46. Mooranian, A., Jones, M., Ionescu, C.M., Walker, D., Wagle, S.R., Kovacevic, B., Chester, J., Foster, T., Johnston, E., Kuthubutheen, J., et al. (2021). Artificial cell encapsulation for biomaterials and tissue bio-nanoengineering: History, achievements, limitations, and future work for potential clinical applications and transplantation.

J. Funct. Biomater. *12*, 68. https://doi.org/10.3390/jfb12040068.

47. Meneghel, J., Kilbride, P., and Morris, G.J. (2020). Cryopreservation as a key element in the successful delivery of cell-based therapies—a review. Front. Med. *7*, 592242. https://doi.org/10.3389/fmed.2020.592242.

48. Lexmond, W., der Mee, J.v., Ruiter, F., Platzer, B., Stary, G., Yen, E.H., Dehlink, E., Nurko, S., and Fiebiger, E. (2011). Development and validation of a standardized ELISA for the detection of soluble Fc-epsilon-RI in human serum. J. Immunol. Methods *373*, 192–199. https://doi.org/10.1016/j.jim.2011.08.018.

49. Dranoff, G. (2002). GM-CSF-based cancer vaccines. Immunol. Rev. *188*, 147–154. https://doi.org/10.1034/j.1600-065X.2002.18813.x.

50. Zhao, W., Zhao, G., and Wang, B. (2018). Revisiting GM-CSF as an adjuvant for therapeutic vaccines. Cell. Mol. Immunol. *15*, 187–189. https://doi.org/10.1038/cmi.2017.105.

51. Vernet, R., Charrier, E., Cosset, E., Fièvre, S., Tomasello, U., Grogg, J., and Mach, N. (2021). Local sustained gm-csf delivery by genetically engineered encapsulated cells enhanced both cellular and humoral sars-cov-2 spike-specific immune response in an experimental murine spike dna vaccination model. Vaccines *9*, 484. https://doi.org/10.3390/vaccines9050484.

52. Suschak, J.J., Bagley, K., Shoemaker, C.J., Six, C., Kwilas, S., Dupuy, L.C., and Schmaljohn, C.S. (2018). The genetic adjuvants interleukin-12 and granulocyte-macrophage colony stimulating factor enhance the immunogenicity of an Ebola virus deoxyribonucleic acid vaccine in mice. J. Infect. Dis. *218*, S519–S527. https://doi.org/10.1093/infdis/jiy378.

53. Nemunaitis, J., Jahan, T., Ross, H., Sterman, D., Richards, D., Fox, B., Jablons, D., Aimi, J., Lin, A., and Hege, K. (2006). Phase 1/2 trial of autologous tumor mixed with an allogeneic GVAX® vaccine in advanced-stage non-small-cell lung cancer. Cancer Gene Ther. *13*, 555–562. https://doi.org/10.1038/sj.cgt.7700922.

54. Potluri, H.K., Ng, T.L., Newton, M.A., and McNeel, D.G. (2022). GM-CSF elicits antibodies to tumor-associated proteins when used as a prostate cancer vaccine adjuvant. Cancer Immunol. Immunother. *71*, 2267–2275. https://doi.org/10.1007/s00262-022-03150-3.

55. Clive, K.S., Tyler, J.A., Clifton, G.T., Holmes, J.P., Mittendorf, E.A., Ponniah, S., and Peoples, G.E. (2010). Use of GM-CSF as an adjuvant with cancer vaccines: beneficial or detrimental? Expert Rev. Vaccines *9*, 519–525. https://doi.org/10.1586/erv.10.40.

56. Parmiani, G., Castelli, C., Pilla, L., Santinami, M., Colombo, M.P., and Rivoltini, L. (2007). Opposite immune functions of GM-CSF administered as vaccine adjuvant in cancer patients. Ann. Oncol. *18*, 226–232. https://doi.org/10.1093/annonc/mdl158.

57. Yan, W.-L., Shen, K.-Y., Tien, C.-Y., Chen, Y.-A., and Liu, S.-J. (2017). Recent progress in GM-CSF-based cancer immunotherapy. Immunotherapy *9*, 347–360. https://doi.org/10.2217/imt-2016-0141.

58. Serafini, P., Carbley, R., Noonan, K.A., Tan, G., Bronte, V., and Borrello, I. (2004). High-dose granulocyte-macrophage colony-stimulating factor-producing vaccines impair the immune response through the recruitment of myeloid suppressor cells. Cancer Res. *64*, 6337–6343. https://doi.org/10.1158/0008-5472.CAN-04-0757.

59. Kumar, A., Taghi Khani, A., Sanchez Ortiz, A., and Swaminathan, S. (2022). GM-CSF: a double-edged sword in cancer immunotherapy. Front. Immunol. *13*, 901277. https://doi.org/10.3389/fimmu.2022.901277.

60. Bhattacharya, P., Budnick, I., Singh, M., Thiruppathi, M., Alharshawi, K., Elshabrawy, H., Holterman, M.J., and Prabhakar, B.S. (2015). Dual role of GM-CSF as a pro-inflammatory and a regulatory cytokine: implications for immune therapy. J. Interferon Cytokine Res. *35*, 585–599. https://doi.org/10.1089/jir.2014.0149.

61. van de Laar, L., Coffer, P.J., and Woltman, A.M. (2012). Regulation of dendritic cell development by GM-CSF: molecular control and implications for immune homeostasis and therapy. Blood *119*, 3383–3393. https://doi.org/10.1182/blood-2011-11-370130.

62. Kaech, S.M., Wherry, E.J., and Ahmed, R. (2002). Effector and memory T-cell differentiation: implications for vaccine development. Nat. Rev. Immunol. *2*, 251–262. https://doi.org/10.1038/nri778.

63. Tai, Y., Wang, Q., Korner, H., Zhang, L., and Wei, W. (2018). Molecular mechanisms of T cells activation by dendritic cells in autoimmune diseases. Front. Pharmacol. *9*, 642. https://doi.org/10.3389/fphar.2018.00642.

64. Förster, R., Schubel, A., Breitfeld, D., Kremmer, E., Renner-Müller, I., Wolf, E., and Lipp, M. (1999). CCR7 coordinates the primary immune response by establishing functional microenvironments in secondary lymphoid organs. Cell *99*, 23–33. https://doi.org/10.1016/S0092-8674(00)80059-8.

65. Seth, S., Oberdörfer, L., Hyde, R., Hoff, K., Thies, V., Worbs, T., Schmitz, S., and Förster, R. (2011). CCR7 essentially contributes to the homing of plasmacytoid dendritic cells to lymph nodes under steady-state as well as inflammatory conditions. J. Immunol. *186*, 3364–3372. https://doi.org/10.4049/jimmunol.1002598.

66. The Gene Ontology Consortium (2019). The Gene Ontology Resource: 20 years and still GOing strong. Nucleic Acids Res. *47*, D330–D338. https://doi.org/10.1093/nar/gky1055.

67. Yoshie, O., and Matsushima, K. (2015). CCR4 and its ligands: from bench to bedside. Int. Immunol. *27*, 11–20. https://doi.org/10.1093/intimm/dxu079.

68. Henry, C.J., Ornelles, D.A., Mitchell, L.M., Brzoza-Lewis, K.L., and Hiltbold, E.M. (2008). IL-12 produced by dendritic cells augments CD8+ T cell activation through the production of the chemokines CCL1 and CCL17. J. Immunol. *181*, 8576–8584. https://doi.org/10.4049/jimmunol.181.12.8576.

69. Suresh, R., and Mosser, D.M. (2013). Pattern recognition receptors in innate immunity, host defense, and immunopathology. Adv. Physiol. Educ. *37*, 284–291. https://doi.org/10.1152/advan.00058.2013.

70. de Wever, B., Kurdykowski, S., and Descargues, P. (2015). Human skin models for research applications in pharmacology and toxicology: introducing NativeSkin ® , the "Missing Link" bridging cell culture and/or reconstructed skin models and human clinical testing. Appl. In Vitro Toxicol. *1*, 26–32. https://doi.org/10.1089/aivt.2014.0010.

71. Robinson, M.D., and Smyth, G.K. (2008). Small-sample estimation of negative binomial dispersion, with applications to SAGE data. Biostatistics *9*, 321–332. https://doi.org/10.1093/biostatistics/kxm030.

STAR★METHODS

KEY RESOURCES TABLE

REAGENT or RESOURCE	SOURCE	IDENTIFIER
Antibodies		
Anti-CD45 Monoclonal antibody [HI30], Alexa Fluor™ 532	ThermoFisher Scientific	58-0459-42
Recombinant anti-CCR7 antibody [Y59], Alexa Fluor 488	Abcam	ab196459
Recombinant anti-CD80 antibody [EPR1157(2)]	Abcam	ab134120
Zenon™ rabbit IgG labeling kit, Alexa Fluor™ 594	ThermoFisher Scientific	Z25307
Anti-human CD83 antibody [HB15e], APC/Cyanine7	Biolegend	305329
Anti-human CD86 antibody [IT2.2], Brilliant violet 650™	Biolegend	305427
Anti-CD40 monoclonal antibody [LOB7/6]	ThermoFisher Scientific	MA1-80926
Zenon™ rabbit IgG2a labeling kit, Alexa Fluor™ 647	ThermoFisher Scientific	Z25108
Anti-human HLA-DR, DP, DQ antibody [Tü39], PE/Cyanine7	Biolegend	361707
Anti-Langerin/CD207 antibody [923B7], Alexa Fluor™ 546	Novusbio	DDX0373A546
Anti-CD1c monoclonal antibody [L161], PerCP-eFluor™710	ThermoFisher Scientific	46-0015-42
Chemicals, peptides, and recombinant proteins		
E. coli-derived human GM-CSF protein	Biotechne R&D systems	215-GMP
RNeasy Plus Mini KIT	Qiagen	74104
Critical commercial assays		
V-PLEX Plus Human GM-CSF Kit	Mesoscale Discovery	K151RIG
V-PLEX Plus Proinflamatory Panel 1 Human Kit	Mesoscale Discovery	K15049G-1
GM-CSF Human ELISA Kit	ThermoFisher Scientific	KHC2011
IgG (Total) Human ELISA Kit	ThermoFisher Scientific	BMS2091
Experimental models: Cell lines		
K562 cells secreting huGM-CSF	This paper	MVX-1
Immortalized human myoblast cells	CCOS	1902
Immortalized human myoblast cells secreting huGM-CSF	CCOS	1901
Immortalized human myoblast cells secreting anti-CTLA-4	This paper	MVX-3
Experimental models: Organisms/strains		
Mouse: C57BL/6NCrl	Charles River	027
HypoSkin XL	Genoskin SAS	HPS004-10
Software and algorithms		
MANTIS software	Genoskin SAS	https://doi.org/10.1101/2023.01.13.523748
Prism 9.5.1	GraphPad	https://www.graphpad.com/scientific-software/prism/
Other		
Monochromated field emission scanning electron microscope	NIST	HELIOS 660
Dynamic tensile and compression test stand	Mecmesin	(Mecmesin Multitest-1)

RESOURCE AVAILABILITY

Lead contact

Further information and requests for resources and reagents should be directed to and will be fulfilled by the lead contact, Julien Grogg (jgrogg@maxivax.ch).

Materials availability

This study did not generate new unique reagents. There are restrictions to the availability of the Myo-P device generated in this study due to the proprietary nature of this technology. Distribution for research purposes is possible under MTA.

Data and code availability

- All data reported in this paper will be shared by the lead contact upon request.
- This paper does not report original code.
- Any reasonable information request related to the data reported in this paper is available from the lead contact.

EXPERIMENTAL MODEL AND STUDY PARTICIPANT DETAILS

Animals

Adult C57BL/6J female mice from 7 to 12 weeks were purchased from Charles River Laboratories (France). Animals were group housed in a specific pathogen-free environment, at 21°C and 29% humidity, with lighting on a 12 h light/dark cycle. Mice were allowed to acclimate for at least 2 weeks before any manipulation. All experiments were performed according to local animal care regulation (Geneva) by trained and licensed personnel. The study protocol was reviewed and approved by the Committee for Animal Research Ethics at the University of Geneva and by the Cantonal Committee for Animal Experimentation, as per Swiss Federal law (study protocol GE/62/20).

Ex vivo human skin model

The HypoSkin model is a validated clinical skin model from Genoskin. It contains living *ex vivo* human skin biopsies with attached subcutaneous adipose tissue harvested from both male and female healthy donors. Gender has no influence on the results of the study provided. The epidermis, dermis, and subcutaneous fat of human origin are embedded in a proprietary solid matrix, with the epidermal surface in direct contact with ambient air, which maintain all tissues alive and fully immunocompetent for more than 7 days[70] Anonymized healthy human skin samples were obtained from donors that underwent abdominoplasty procedures and had given their written informed consent. Donors did not have any record of allergies or dermatological disorders and did not use corticosteroids. Genoskin has obtained all legal authorizations necessary from the French Ministry of Higher Education, Research and Innovation (AC-2017-2897) and the Personal Protection Committee (2017-A01041-52). All studies were conducted according to Declaration of Helsinki protocols.

Media and reagents

The medium used for the culture of all myoblast cell lines is a customized growth medium (GM) prepared with Ham's F-10 Nutrient Mix GlutaMAX Supplement (Gibco, 41550021) and supplemented with 15% FBS, 0.5 mg/mL bovine serum albumin (BSA) (Sigma Aldrich, A4503), 0.5 mg/mL fetuin (Desert Biological, 302070), 10 ng/mL epidermal growth factor (R&D Systems, 236-GMP-200), 0.39 μg/mL dexamethasone (PharmaServ, 8016), 0.04 mg/mL insulin (Sigma Aldrich, I9278), 149 μg/mL creatine monohydrate (PharmaServ, 8114), 100 μg/mL pyruvate (Gibco, 11360039), 50 μg/mL uridine (Sigma Aldrich, U3003) and 5 μg/mL gentamycin (Gibco, 15710049).

METHOD DETAILS

Device manufacturing

The manufacturing process of both the GEN-1 and the Myo-P devices was developed and supported by feasibility assessments, parameter optimization, scale-up trouble shooting, and engineering batches. Both devices have essentially two parts: a semi-permeable HFM reinforced by a stainless steel helicoid coil, and a retrieval tube on the proximal end of the device. Both the GEN-1 and the Myo-P devices were prepared with a 13 mm (+/− 0.5 mm) long HFM section (ID 0.7 mm) and were assembled according to the description presented in Figures 1A–1C). The characteristics of both the GEN-1 and the Myo-P HFMs are described in Table S1. Due to the design and material specifications of the capsule, the sterilization process is performed with ethylene oxide (EO) at 55°C. The capsules go through a degassing phase to

allow for adequate EO desorption. After sterilization, biological indicators are analyzed to validate the sterilization process.

Mechanical characterization

The samples were characterized by different analytical techniques. Scanning electron microscopy (SEM) was performed by using a monochromated field emission scanning electron microscope (HELIOS 660). Tension at break and transmembrane flow pressure were performed using a dynamic tensile and compression test stand (Mecmesin Multitest-1) with a 10N calibrated cell. Membrane tension at break was assessed on 13-mm (+/− 0.5 mm) long HFM sections (n = 20) in each group, with a traverse speed set at 2 mm/s. Transmembrane flow pressure was assessed by injecting HTF culture medium with 10% albumin in 13-mm (+/− 0.5 mm) long HFM sections (n = 3) with a traverse speed set at 2 mm/s. The sections of membrane used in this experiment were obstructed with a UV-curable adhesive (Dymax MD1187). Elasticity was assessed by applying an angulation to 13-mm (+/− 0.5 mm) long HFM sections until plastic deformation (n = 5).

Cell encapsulation

All cell lines were cultured in T-Flasks at a defined density (cell/cm^2), in a defined volume of culture medium and incubated for 24 h as described above. Given the adherent nature of the MVX-2 (human GM-CSF-secreting cells/Culture Collection Of Switzerland (CCOS) 1901) and the MVX-3 (anti-human CTLA4 antibody-secreting cells) human myoblast cells, a trypsinization process was required to pass and count cells. All cell lines were counted in duplicate with an automated cell counter (Countess II device, Thermo Fisher Scientific) and resuspended in culture medium. Each capsule was loaded with 30 μL of the cell suspension containing 1 M of cells through a loading tube (vasculon). After loading, the vasculon was cut and capsules were sealed with UV-curable adhesive (GEN-1 device with Dymax MD1180, and Myo-P capsules with MD1187). Capsules were placed in 12-well plates containing 2 mL of culture medium per well and maintained in a humidified incubator with 5% CO_2 at 37°C.

Freezing and thawing of loaded Myo-P capsules

Before freezing, capsules were loaded using the same procedure previously described, except that the cells were resuspended in freezing medium (culture medium supplemented with 10% glycerol (Sigma Aldrich, 49767)) instead of normal culture medium. Capsules were then placed in silicone tubes prefilled with freezing medium, and the latter were subsequently transferred into cryotubes. Cryotubes were immediately placed in a CoolCell freezing chamber (Corning) and frozen at −80°C overnight, then stored in liquid nitrogen. Capsules were thawed by placing the frozen silicone tube in which they were contained into a 10-cm Petri dish filled with pre-warmed (37°C) culture medium immediately after being taken out of liquid nitrogen. Then, capsules were removed from the silicone tubes and placed in 12-well plates containing 2 mL of culture medium and maintained in a humidified incubator with 5% CO_2 at 37°C.

Implantation of capsules in mice

Adult mice received a subcutaneous injection of 0.1 mg/kg buprenorphine for analgesia 20 min before anesthesia. Afterward, mice were anesthetized with isoflurane and a capsule was implanted in the subcutaneous tissue of the flank in each mouse using a trocar. The wound was sutured with surgical staples and animals recovered in their home cage. After surgery, analgesia was provided with 2 mg/mL acetaminophen added to the drinking water for three days. At sacrifice, blood was collected by terminal cardiac puncture under anesthesia with xylazine and ketamine. The tissue around the capsule was snap frozen in liquid nitrogen. Capsules were dissected and retrieved from the mice and were placed in culture medium for further quantification of Protein of Interest and then fixed for further histological analysis.

Implantation in an ex vivo human skin model

The HypoSkin models were mounted on cell culture inserts, loaded in multi-well companion plates with lids containing proprietary medium. This medium was free of serum, growth factors, phenol red, or hydrocortisone. The plates were then kept at 37°C with 5% CO_2. Capsules were implanted between the hypodermis and the dermis using a 14G catheter (BD Insyte SKU 381467), and biopsies were collected at different timepoints.

Tissue preparation

Punch biopsies were mechanically dissociated in gentleMACS M Tubes (Miltenyi Biotech, 130-093-236) using the GentleMACS protein program. Tissue samples were processed in 500 μL of T-PER Tissue Protein Extraction Reagent (Thermo Fisher Scientific, 78510) and cOmplete, Mini, edetic acid (EDTA)-free Protease Inhibitor Cocktail Tablets (Sigma Aldrich, 04693159001). After dissociation, samples were centrifuged, and the supernatant was collected and analyzed for protein quantification.

Protein quantification

All recombinant protein secreted by encapsulated cells, as well as their presence in the blood or in the tissue of animal and human models were quantified by immunoassay. After cell encapsulation and maintenance, capsules were transferred into 12-well plates containing 2 mL of fresh culture medium and maintained in a humidified incubator with 5% CO2 at 37°C for 2 to 24 h. The medium was then collected for analysis. Results were reported in ng/24 h/capsule. Tissue lysates of human origin were analyzed with the V-PLEX Plus Human GM-CSF Kit (Mesoscale Discovery, K151RIG) and the V-PLEX Plus Proinflamatory Panel 1 Human Kit (K15049G-1), and results were reported in pg/125 μg total protein. Tissue lysates of murine origin were analyzed with the GM-CSF Human ELISA Kit (Thermo Fisher Scientific, KHC2011), and results were reported in pg/mg total protein. Antibodies were quantified with an IgG (Total) Human ELISA Kit (Thermo Fisher Scientific, BMS2091). All protocols were applied according to the manufacturer's instructions.

Multiplexed imaging

For imaging purposes, 40 μm OCT tissue sections were blocked and permeabilized with PBS, 0.5% BSA, 0.3% Triton X-100 at room temperature, then incubated with fluorophore-coupled antibodies overnight at 4°C in the dark. The sections were then washed three times in PBS, 0.5% BSA, 0.3% Triton X-100. Finally, samples were treated with an autofluorescence quenching solution. The slides were mounted in Mowiol medium and sealed with a coverslip. z stack images with a resolution of 512x512 pixel were acquired using a confocal microscope SP8 (Leica Microsystems). 3D mosaic images were then imported into Huygens SVI software in order to correct the signal by applying deconvolution and crosstalk correction. 3D mosaic images were imported into Imaris software and a segmentation was applied on the CD45 channel surface. Statistical properties (Object Volume, Sphericity, Area, xyz Position and Mean Fluorescence Intensity) were exported as a.csv table. Each object was then phenotypically assigned to a cell type based on biomarkers expression using the MANTIS software (Genoskin SAS). Visualization charts were obtained using the ggplot2, Pigengene & Complex Heatmap R packages, and matplotlib & seaborn Python packages. t-Distributed Stochastic Neighbor Embedding (tSNE) was computed with Rtsne.[38] Experimental workflow along with APCs panel is described Figure S2.

Skin bulk RNA sequencing

RNA extraction was made using the RNeasy Plus Mini KIT (Qiagen #74104). Libraries were produced using TruSeq Stranded mRNA Illumina and their quality was assessed using a fragment analyzer. FastQ files were generated via 2x150 bp Flowcell SP on Illumina NovaSeq. Quality of FastQ files was controlled using FastQC and trimmed with TrimGalore. Reads were aligned with *Homo sapiens* transcriptome reference GRCh38 using STAR. Then reads were sorted with SAMtools. The quantification of gene expression was performed with HTSeq2. Filtering, normalization, and differential expression analysis was done using the R package EdgeR. The library size was normalized with the TMM method. Filtering and data normalization were performed by calculating the log2(cpm). Only log2(cpm) > −1 were conserved. The differential gene expression analysis was performed using the exact test of Robinson and Smyth (2008) for a difference in mean between two groups of negative binomial random variables.[71] The Bonferroni method was used for adjusting p values and only genes with an adjusted p value <0.05, a logFC >1 and a false discovery rate (FDR) < 0.05 were kept. R Pheatmap package was employed to display differentially expressed genes (DEGs) (hierarchical clustering using the euclidean distance and complete linkage method). Pathway analysis was performed with the R package EnrichR using the Gene Ontology database.[39,40]

QUANTIFICATION AND STATISTICAL ANALYSIS

Results are expressed as mean ± standard deviation. Statistical significance was assessed by Student's *t* test for comparison between two groups, and two-way analysis of variance (ANOVA) followed by Tukey's multiple comparison test. Statistically significant differences between groups is presented as follows: *p < 0.05,

**p < 0.01, ***p < 0.001 and ****p < 0.0001. Area under the curve (AUC) is presented as total area of arbitrary units, standard error, and 95% Confidence Interval (CI). Box, whiskers, and violin plots were created to illustrate range (min-max). Data analyses were performed using the software package GraphPad Prism 9 (GraphPad Software).

ADDITIONAL RESOURCES

The MVX-ONCO-1 trials referred in this article are registered at Clinicaltrials.gov registration NCT02193503 and NCT02999646.